REVISTA DE METALURGIA, 46 (4)
JULIO-AGOSTO, 308-319, 2010
ISSN: 0034-8570
eISSN: 1988-4222
doi: 10.3989/revmetalm.0911

Analysis of rail cooling strategies through numerical simulation with instant calculation of thermal expansion coefficient(•)

A. Pernía-Espinoza*, F.J. Martínez-de-Pisón*, E. Martínez-de-Pisón* and J. Blanco*

Abstract

This article describes a new methodology to simulate the cooling process for an asymmetrical Ri60 grooved rail, designed for city tramways, in a more realistic manner than that conducted previously by other authors for long steel sections. The approach considers the phase transformation of the steel and the forced convection cooling. The process is modelled as an uncoupled thermo-mechanical problem. First, the rail's temperature history is obtained from a computer fluid dynamic model and subsequently introduced in the finite element model, in order to model the stresses and displacements. This second stage involves the calculation of the thermal expansion coefficient, for each element and at each iteration. The calculation is made according to the continuous cooling transformation diagram. These results lead to the extremely reliable determination of residual stresses as proved by the comparison with experimental data obtained in the industrial plant. The methodology allows for an accurate study of two types of cooling strategies for the Ri60 and the selection of the more suitable one.

Keywords

Residual stresses; Section manufacturing; Thermal expansion coefficient.

Análisis de estrategias de enfriamiento de raíles mediante simulación numérica con cálculo instantáneo del coeficiente de expansión térmica

Resumen

En este artículo se describe una nueva metodología para simular el proceso de enfriamiento de un rail asimétrico Ri60, diseñado para tranvías, de una forma mucho más realista que lo realizado hasta ahora para perfiles largos de acero. La propuesta considera los efectos de la transformación de fases del acero y el enfriamiento por convección forzada. El proceso es simulado como un proceso termo-mecánico desacoplado. Primero, las curvas de enfriamiento del rail son obtenidas a partir de un modelo basado en dinámica de fluidos computacional y posteriormente introducidas en el modelo de elementos finitos para calcular las tensiones y desplazamientos. En esta segunda fase se calcula, para cada elemento finito y en cada iteración, el coeficiente de dilatación térmica lineal según el diagrama de curvas de enfriamiento continuo. Estos resultados permiten determinar las tensiones residuales al final del proceso con muy buena fidelidad respecto a los datos experimentales obtenidos en la planta industrial. La metodología permite estudiar con precisión dos tipos de estrategias de enfriamiento del Ri60 y seleccionar la más conveniente.

Palabras clave

Tensiones residuales; Fabricación de perfiles; Coeficiente de dilatación térmica lineal.

1. INTRODUCTION

Residual stresses produce significant effects on the carrying capacity of steel beam columns within a structure[1]. Furthermore, it has been reported by many authors that residual stresses influence the mechanical behaviour of structural material and, consequently, lead to the propagation of cracks in the case of rails[2-7]. Residual stresses in rails can cause plastic deformation around the rail-wheel contact surface and modify the stress field near the running line and internally in the railhead causing railway failures[8].

Along the manufacturing process of steel long product, the cooling process is the first stage in which the residual stresses start to appear. Depending on cross-section shape and thickness, the section starts to cool down at different rates, and this is when thermal stresses appear. At the beginning of the cooling process, temperatures in the section are very high and the thermal stresses could be higher than the material's

(•) Trabajo recibido el día 6 de Marzo de 2009 y aceptado en su forma final el día 13 de Abril de 2010.
* EDMANS Group (http://www.mineriadatos.com), Department of Mechanical Engineering, Universidad de La Rioja, Spain. + 34 941 299 517; Fax: + 34 941 299 794. E-mail address: *alpha.pernia@unirioja.es.*

yield stress. These conditions cause plastic deformations, with the consequent bending and development of residual stresses. The residual stresses are subsequently modified during the straightening process. However, the inherit temperature and stress profiles from the cooling process can affect the straightening process. The most critical situation would be an excessive bending that does not allow the section to be introduced into the straightening machine.

In the final product, residual stress is one of the more important factors affecting fracture failure. It is also a parameter that can be controlled and reduced during the manufacturing process through effective strategies. To be able to propose improvements in this area, it is necessary to model and analyse the processes involved, and finite element (FE) analysis and computational fluid dynamics (CFD) are two versatile tools for achieving this goal[9 and 10].

This work focused on the modelling and simulation through CFD and FE models of the rails' cooling process. The main objective was to study the evolution of temperature and stresses during the cooling process in order to explain the residual stress profile and bending of the product.

This paper is the result of a European research project in which steel section producers have joined forces with research institutions to analyse and improve their manufacturing processes. Thanks to the steel companies involved in the project, valuable experimental data were forthcoming for comparison with the simulation and for model calibration.

The next section briefly describes the state-of-the-art in cooling process simulations using numerical simulation. This is followed by an explanation of the methodology applied and the CFD and FE models development. The results of the simulations and a comparison with experimental data are then presented. In the final section, conclusions and further research lines are drawn.

2. RELATED RESEARCH WORK

In the 1980s-1990s, the problem of reducing residual stresses in rails was addressed by almost all the world's rail-producing firms. Residual stress was adjudged to be a secondary variable in the first theoretical investigations into detail fatigue crack propagation[11]. However, later correlations of full-scale tests, stress measurements and rail failure reports with a similar model showed that residual axial tension in the rail head has a major effect on detailed fracture propagation life[12].

As a consequence, measuring and modelling thermal stress during the continuous cooling of hot-rolled products have received significant attention in recent years. Most of the initial research was experimental, with verifications based on quite simplified theoretical models[13]. Later on the author of [14 and 15] were the first to analyse residual stresses in hot-rolled complex beams using a finite element method. Their work was preceded by those of other authors[16-18] who studied thermal stress formation in engineering problems, using a two-dimensional thermo-elastic finite element idealization. However, the verification of the methods with experimental values was not clear.

Fisher *et al.*[18] studied residual stress distribution in rails during cooling by taking into account the friction with the supports. They dismissed the assumption that residual stresses are constant over the whole length, except for a small end part in the range of approximately two beam heights. They also pointed out that frictional forces between the rail and supports have some influence on the residual stress state. Ringsberg and Lindbäck[3] arrived to a stress distribution on a rail after cooling based also on a two dimensional FE model. Nevertheless, the final stress distribution does not seem to agree with the one reported in the literature (maximum tensile stress values at rail's head and foot center). Basu *et al.*[19] produced a finite element model of rail cooling with results close to reality. The problem was investigated in a three-dimensional model of the rail, and as a decoupled thermo-mechanical transient problem, using ANSYS® for both the thermal and the structural analysis. They also considered the influence of the surrounding rails on the cooling bed. Nevertheless, the bending of the rail was assumed to be in the form of a circular arc, which is not always true (Fig. 1). In addition, the film heat transfer coefficient was calculated for ideal conditions and modified throughout the process to achieve the real cooling rate. Boyadjiev *et al.*[20] used a plane-strain FE analysis for the computational prediction of deflection and residual stress in the cooling of hot-rolled beams. The analysis was based on the generalized plane-strain model of Abouaf *et al.*[14]. They include contact with the supporting table and the effect of beam weight. Their main contribution was to represent the beam's thermal expansion coefficient as a function of temperature, cooling rate and phase transformation kinetics. No clear agreement was found between simulation results and experimental measurements regarding the rail cooling model.

It is important to point out that all the references found, related to residual stress formation during rail cooling, were developed for symmetrical cross-section rails (UIC-section rails). Grooved rails, like the one studied here, pose a greater challenge because of their lack of symmetry about an axis.

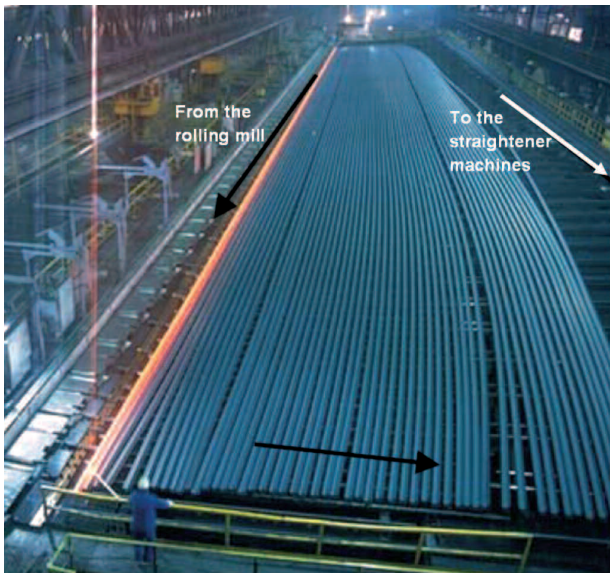

Figure 1. Cooling bed studied. Courtesy of Voestalpine Stahl Donawitz GmbH & Co KG.

Figura 1. Mesa de enfriamiento estudiada. Cortesía de Voestalpine Stahl Donawitz GmbH & Co KG.

3. DESCRIPTION OF THE PROBLEM

The cooling process, after the hot rolling mill, is the phase in steel section manufacturing in which residual stresses start to appear. Researches have shown that final bending and residual stresses after cooling are related to the performance of the rails after the straightening process.

Cooling processes in manufacturing of steel long products are basically very similar. In general, the cooling bed is a framework of carbon steel beams parallel to each other. Some of these beams are fixed and others are moveable (walking beams) to facilitate the transportation of the rails. A picture of the cooling bed modelled is shown in figure 1.

The rail comes from the hot rolling mill at high temperatures (around 1,000 °C), passing over the ingoing roller table to the cooling bed. Once there, the section moves through the cooling bed, helped by the walking beams, till it reaches a suitably lower temperature to be sent to the next process – the straightening. The rail output temperature is about 30 °C. To reach this value, the rails are cooled for approximately three hours. The wind magnitude and direction over the cooling bed could influence the resulting residual stresses profile.

A common assumption is that the section leaves the last rolling mill under no state of stress because of the high temperatures[15].

An important characteristic of the cooling bed studied is that it is located indoors and, according to the layout, air flows largely in one direction. Figure 2 shows a general description including the main wind direction (east-west). Air flow conditions were measured with rails on the cooling bed, and the magnitude obtained in the prevailing direction was 1.5 m/s.

The rails are cooled one by one on their way to the straightening process. Two main positions were considered for the rails on the cooling bed: vertical and horizontal (Fig. 3).

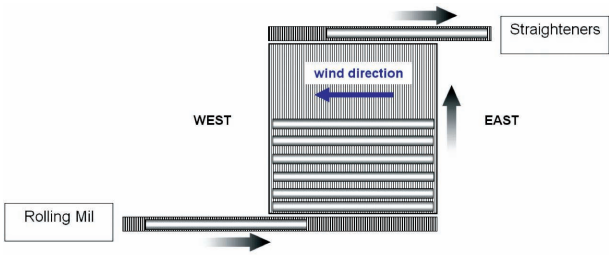

Figure 2. General cooling bed configuration. The principal wind direction is 'East-West'.

Figura 2. Configuración general de la mesa de enfriamiento. La dirección principal del viento es 'Este-Oeste'.

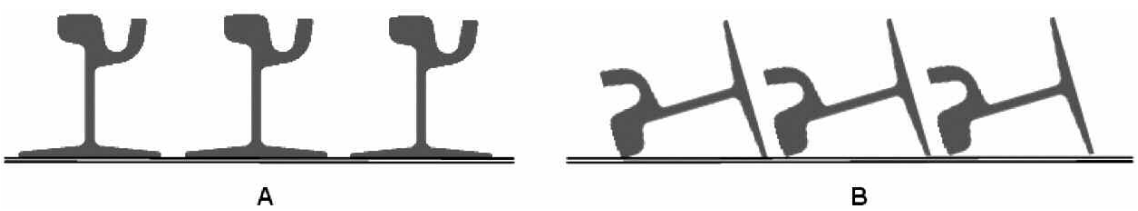

Figure 3. Rails' configuration strategies simulated. A. Standing position, B. Lie-down position.

Figura 3. Estrategias simuladas respecto a la posición de los raíles. A. Posición vertical, B. Posición horizontal.

The horizontal configuration (B) is the one normally used in plants to avoid the 'domino' effect. Nevertheless, the study of the residual stress development in both arrangements was deemed to be of interest.

Experimental values for comparison with the simulation of the models were kindly provided by the company. The temperature trend during the cooling process was measured at certain interesting surface points using NiCrNi-thermocouples of 1.5mm in diameter. The thermocouples were located at 1.5 m from the rail's end. Residual stresses were measured after the rail was cooled in a vertical position, using the sectioning method: 20mm thick pieces were cut from a 1 m central rail section.

4. CFD AND FE MODELS OF THE COOLING PROCESS

The modelling of the cooling process was divided into two parts: one for thermal behaviour and the other for stress/displacement behaviour. As mentioned earlier, this was possible because the type of thermo-mechanical problem studied is such that the thermal evolution of the problem affects the stress response, but the temperature field does not depend on the stress field. Consequently, the temperature trend can be calculated in a decoupled thermal analysis and then introduced as a predefined field in the stress/displacement analysis. First, the model for configuration A (rail-by-rail cooling in a vertical position) is presented. Subsequently, next section draws a comparison between the results for both configurations, A and B (horizontal position).

4.1. CFD thermal model

The thermal model for the grooved rail cooling process was designed using FLUENT® software[21].

The model included the following characteristics:

— Rail cooling was simulated by means of the heat transfer through forced convection and radiation into the air flow.
— The model caters for the influence of the surrounding rails on the cooling of the rail studied: heat from the rails located at both sides.
— The model included the boundary conditions related to wind magnitude and direction: 1.5m/s in 'East-West' direction. These data were obtained from the real cooling bed.
— The Ri60 rail simulated was 5m in length (long enough to avoid border effects and enable us to perceive the rail's bending during the process). Meshing was based on 3D hexahedral elements. The element length in the rail's direction was 62.5 mm
— The steel studied was the EN200.

Once the thermal simulation process had been completed in FLUENT®, the cooling curves (temperature-time) were obtained for each one of the rail's mesh elements.

4.2. FE-stress/displacement model

In order to analyse the stresses and deformations produced by temperature changes, the sequentially coupled thermal-stress analysis adopted required a conversion code. Through this code was possible to communicate the temperature results of the thermal model (formulated in FLUENT®) to the FE-stress/displacement model, created in ABAQUS®. The conversion code was created using freeware (Linux shell programming by means of awk scripts; R® and C programming by means of gcc) in a simple and computationally efficient way.

In order to render the FE-stress/displacement model much more accurate, a methodology was designed that allowed for determining the thermal expansion coefficient (α_{th}) as a function of time and for each finite element in the model. The methodology to calculate this important coefficient was based on a function that was dependent on time, temperature and the proportions of the material's austenite and ferrite phases at each moment. This required determining the cooling curves of the different parts of the grooved rail and transferring them to the "Continuous Cooling Transformation" (CCT) diagram of the EN200 (Fig. 4).

From the CCT curves the percentage and type of transformation product can be found. For the hypo-eutectoid steel used for the rails, the phase transformation region comprises two phases: ferrite and austenite. Therefore, the thermal expansion coefficient can be given as a mean value, weighted according to the fraction of ferrite and austenite present during the perlite reaction[22]:

$$\alpha_{th} = \alpha_{th,\,ferrite} \cdot X + \alpha_{th,austenite} \cdot (1 - X) \qquad (1)$$

where, X is the "volume fraction of intended phase at T temperature".

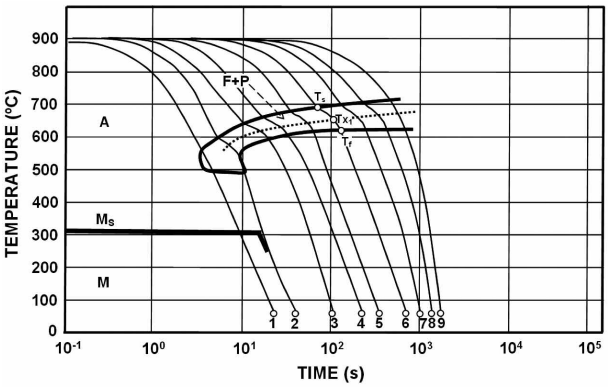

Figure 4. Continuous cooling transformation diagram (CCT) of an EN200 steel austenitised at 900ºC for 14 min.

Figura 4. Diagrama de transformaciones en enfriamiento continuo (CCT) del acero EN200, austenizado a 900ºC por 14 min.

The process for calculating α_{th}, according to Boyadjiev *et al.*[22], was based on the determination of X in the multiphase region. using a numerical method involving the equation by Kamamoto *et al.*[23]:

$$X = X_0\left\{1-\exp\left[-b\left(\frac{T_s-T}{T_s-T_f}\right)^n\right]\right\} \qquad (2)$$

where,

- X is the "volume fraction of intended phase at T temperature",
- X_0 is the "volume fraction of intended phase at transformation termination",
- T_s is the transformation start temperature,
- T_f is the transformation finish temperature, and
- n, b are constant values.

Out of the multiphase region, it is considered that the perlite reaction is not started when $T>T_s$ and consequently X = 1. In the same way, when $T<T_f$, it is assumed that the reaction is completed and therefore X = 0.

Considering now the CCT diagram displayed in figure 4, if X_1 and X_2 are two known volume fractions of the multiphase zone, for and respectively, equation (2) gives:

$$X_1 = 1-\exp(-b\tau_1^n) \qquad (3)$$

$$X_2 = 1-\exp(-b\tau_2^n) \qquad (4)$$

where, $\tau_1 = \dfrac{T_s-T_{X_1}}{T_s-T_f}$ and $\tau_2 = \dfrac{T_s-T_{X_2}}{T_s-T_f}$

The following relations can be obtaining from solving equations (3) and (4) for n and b:

$$n = \frac{\ln\left[-\ln(1-X_1)\right]-\ln b}{\ln\tau_1} \qquad (5)$$

$$b = \exp\left\{\frac{(\ln\tau_1)\cdot\ln\left[-\ln(1-X_2)\right]-(\ln\tau_2)\cdot\ln\left[-\ln(1-X_1)\right]}{\ln\tau_1-\ln\tau_2}\right\} \qquad (6)$$

Each cooling curve of the CCT diagram will gives a specific n and b.

Generally, it is difficult to obtain both references in the majority of the CCT diagrams. From most of the CCT only one X for a given T it is provided (i.e. the values of X_1 and T_{X1}). Nevertheless, it can be assumed that point 2 is located near the end of the decomposition of austenite to perlite. Accordingly, for each cooling curve we will take X_2 = 0.9999 for a temperature $T_{X2} = T_f + 1$ °C. The sensitivity of this assumption was checked in[22] with acceptable results.

Therefore, for given temperature and a specific cooling curve, the thermal expansion coefficient can be defined by (1):

$$\alpha_{th} = \alpha_{th,ferrite}\cdot X + \alpha_{th,austenite}\cdot(1-X)$$

where:

$$\begin{aligned} X &= 1 && \text{if } T > T_s \\ X &= 1-\exp\left[-b\cdot\left(\frac{T_s-T}{T_s-T_f}\right)^n\right] && \text{if } T_f > T \geq T_s \\ X &= 0 && \text{if } T \leq T_f \end{aligned} \qquad (7)$$

and the constants $\alpha_{th,ferrite}$ and $\alpha_{th,austenite}$ are obtained from dilatometric experiments. In the case of the rail steel used in this paper these values were 1.53e–5 °C^{-1} and 2.00e–5 °C^{-1} for $\alpha_{th,ferrite}$ and $\alpha_{th,austenite}$ respectively.

According to this methodology, before starting to calculate the FE-stress/displacement model, prior work have to be undertaken. It is necessary to obtain b and n values for each one of the nine cooling curves in figure 4, using equations (5) and (6).

Afterwards, for each element in the model, a cooling curve was obtained directly from the thermal model. Each of these cooling curves was classified according to the nearest to the original nine cooling curves in the CCT diagram (see figure 4). The classification was possible through the calculation of

the "dissimilarity"[24] between two curves. In this case, the "dissimilarity" was calculated between each of the finite element cooling curve against each of the CCT cooling curves, in the time interval from 10 to 600 s. The two curves compared were divided in vertical segments. The *dissimilarity* was checked between the curves' segments and was calculated considering the shape they take over time, but independently of their length. Therefore, given two vertical segments, $X(t)$, from the element cooling curve, and $Y(t)$, from the CCT cooling curve, of lengths L_x and L_y respectively, the calculation of "dissimilarity" can be defined as:

$$DIS_{Shape} = \frac{\sum_{i=0}^{N} d(X_i, Y_i)}{N+1} \qquad (8)$$

with N being the number of divisions made in each one of the segments and $d(X_i, Y_i)$ the Euclidean distance between X_i and Y_i points. Figure 5 explains these concepts.

Once the "dissimilarity" between the cooling curves has been determined for each one of the elements, a table was used to store the closest curve into the CCT diagram that corresponds to each one of the finite elements' cooling curves.

Once the process was under way for calculating the FE-stress/displacement model in ABAQUS® and, at each iteration and for each finite element, α_{th} was determined on the basis of the n and b coefficients of the corresponding curve and its temperature at that moment. The algorithm was implemented through the *UEXPAN* sub-routine in ABAQUS® that allows for specifying α_{th} at each moment and for each element[25].

Furthermore, the FE-stress/displacement model presented the characteristics listed below:

- The contact between the rail and the cooling bed's supports was considered. The frictional coefficient was set to 0.1.
- The gravity forces (9.81m/s^2) were included.
- The mesh of the section was exactly the same as for the thermal model, in order to facilitate the task of the conversion code (the code that converts the temperature results to be read by the mechanical model).

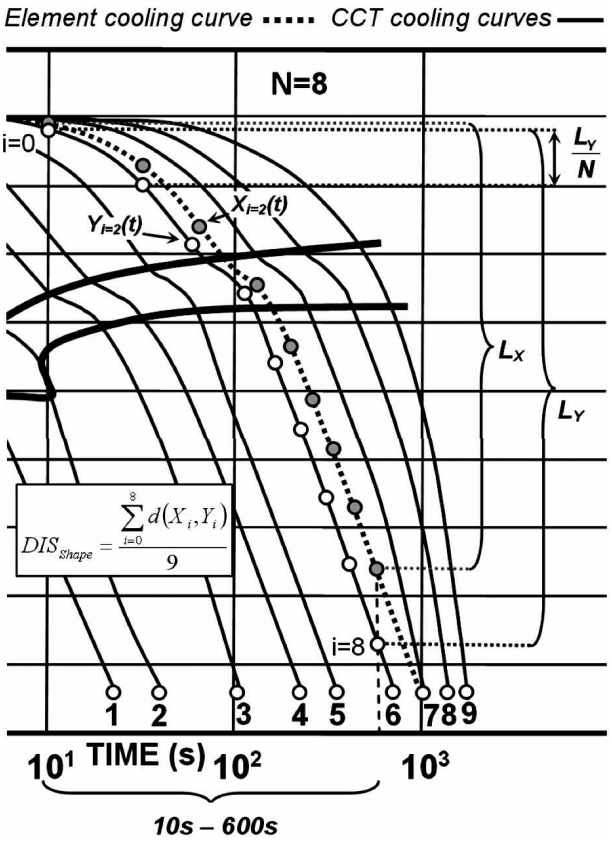

Figure 5. Example of points selection for the calculation of dissimilarity between an element cooling curve and diagram CCT cooling curve number 6.

Figura 5. Ejemplo de selección de puntos para el cálculo de la disimilitud entre una curva de enfriamiento de un elemento y la curva de enfriamiento número 6 del diagrama CCT.

5. RESULTS

5.1. Results of thermal model simulations

The temperature trend recorded by the CFD model was very similar to the experimental one. The comparison for the rail head surface can be seen in figure 6.

At the end of cooling, it was also possible to observe the non-uniform temperature distributions between the windward part of the beam (East facing) and the leeward part (West facing). As logical, the windward part cools faster than the leeward part. The effect of this asymmetrical cooling on residual stresses was also studied.

5.2. Results of stress/displacement model simulations

Figure 7 presents the computed and experimental final stresses values for ten control points. As can be seen, there was consistency between simulated and

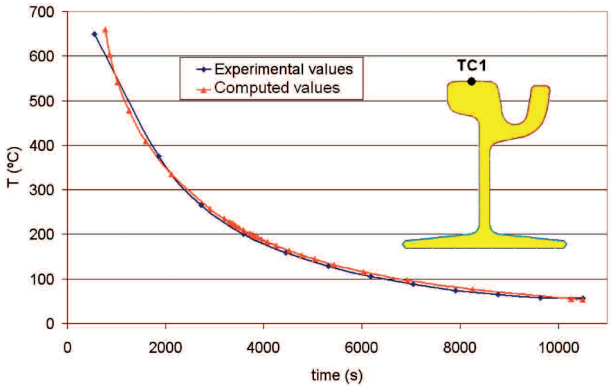

Figure 6. Comparison of computed and experimental values of the temperature history for the head-surface in vertical position.

Figura 6. Comparativa de los valores calculados y experimentales de la evolución de la temperaturas en la superficie de la cabeza en posición vertical.

experimental values, in both, in nature (compression-tension) and also in magnitude.

It is important to point out that it is difficult to obtain accurate experimental values in the areas related to points 4, 5 and 6, as they are not easy to access through the measuring method. The method used (sectioning method, specified for rails, following EN13674-1) also has a tolerance of about ±25 MPa. Accordingly, the differences between experimental and computed values were acceptable.

The residual stresses formation along the time, at the surface and inside the rail's cross-section (at the rail centre section), is displayed in the following figures (8, 9, 10 and 11). Also the bending of the rail on the main planes is displayed. From figure 11, one can observe that the highest tension residual-stresses were located in the rail's big-head centre and in the rail's base-centre. The largest compression residual-stresses were located at the base-tip corresponding to the big-head side and also at the top of the small-head.

Through the observation of the longitudinal stresses (S33 in Pa), temperature (NT11 in °C) and deformation during cooling, it is possible to explain the residual stress profile after cooling. The main observations are shown below.

— S33 changed from compression (–), at the beginning of the cooling process, to tension (+), at the end of the process.

— At the beginning of the cooling process (Fig. 8), the rail's base-tips, web and small-head-tip (which are the parts with a larger external surface) cooled and shrank faster than the parts with more material inside, such as the big-head. These parts therefore tended to pull the rail's base-centre and big-head, and, as a reaction, they contracted. As a consequence, compression stresses are observed in these parts. Points where the stresses reached the yielding stress (which is low for high temperatures) suffered plastic deformation.

— At the final phase of the cooling process (Figs. 10 and 11), the base and web reached a more uniform temperature and it was the big-head and base-centre that started to cool down at a faster rate. This caused the opposite reaction than before: compression stresses in the web, base-tips and small-head-tip, and tension stresses in the big-head and base-centre.

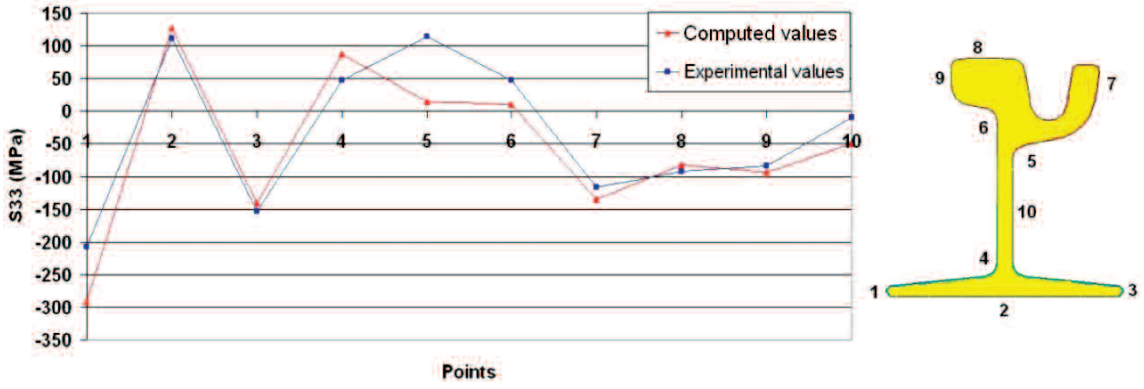

Figure 7. Comparison of computed and experimental residual stresses for 10 interesting surface points on the rail after cooling (t = 10000 s).

Figura 7. Comparativa de los valores calculados y experimentales de las tensiones residuales de 10 puntos superficiales de interés en el rail luego del enfriamiento (t = 10000s).

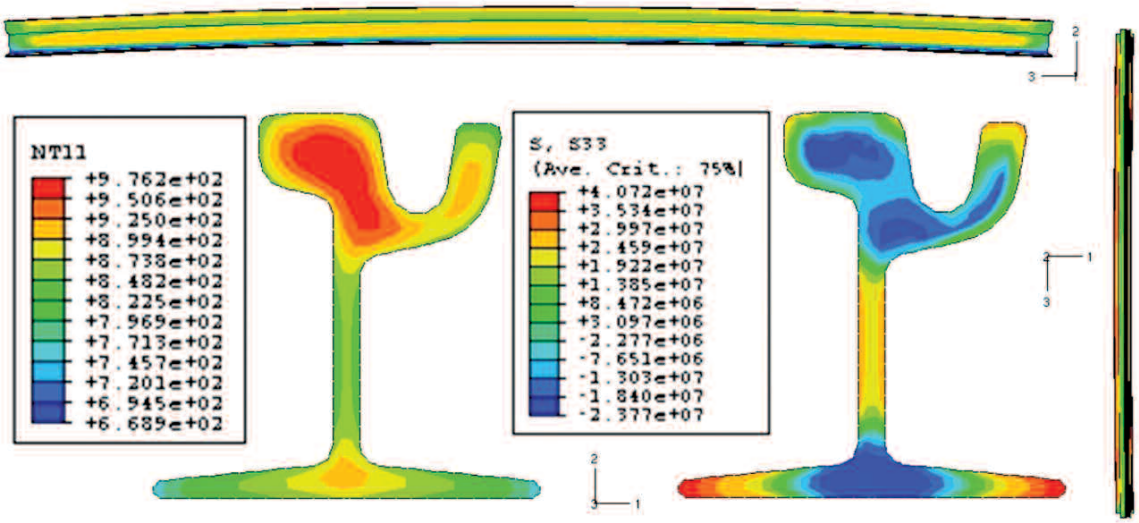

Figure 8. Stresses (S33 in Pa), displacements behavior and temperatures (NT11 in ºC) at the beginning of the cooling process (t = 32 s).

Figura 8. Tensiones (S33 en Pa), comportamiento de los desplazamientos y temperaturas (NT11 en ºC) al inicio del proceso de enfriamiento (t = 32 s).

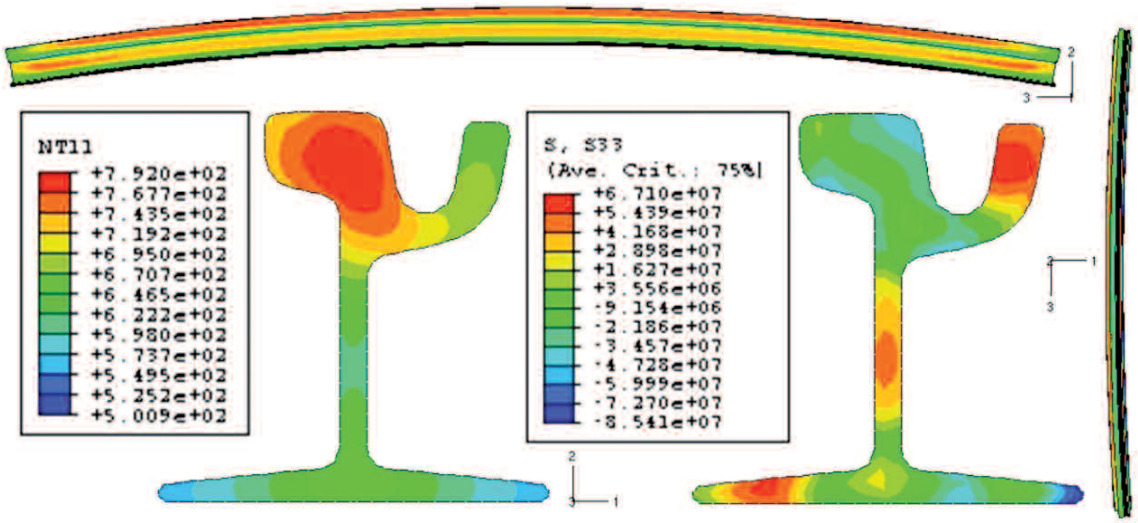

Figure 9. Stresses (S33 in Pa), displacements behavior and temperatures (NT11 in ºC) at time 152 s.

Figura 9. Tensiones (S33 en Pa), comportamiento de los desplazamientos y temperaturas (NT11 en ºC) a los 152 s.

— Regarding bending, it can be said that as the base and the small-head were the parts of the rail that cooled faster at the beginning of the process, the rail bent around these parts (around the base and around the small-head). See figure 9. Later on, these parts reached a more uniform temperature and it was the big-head that started to cool down more quickly, causing the bending around it. This is the final bending observed in the real cooling bed.
— In this case, because of the asymmetry of the section, the residual stresses had a non-symmetric distribution in the base.

To conclude, we can say that the cooling rate, residual stresses and bending of the rail closely follow experimental observations and values.

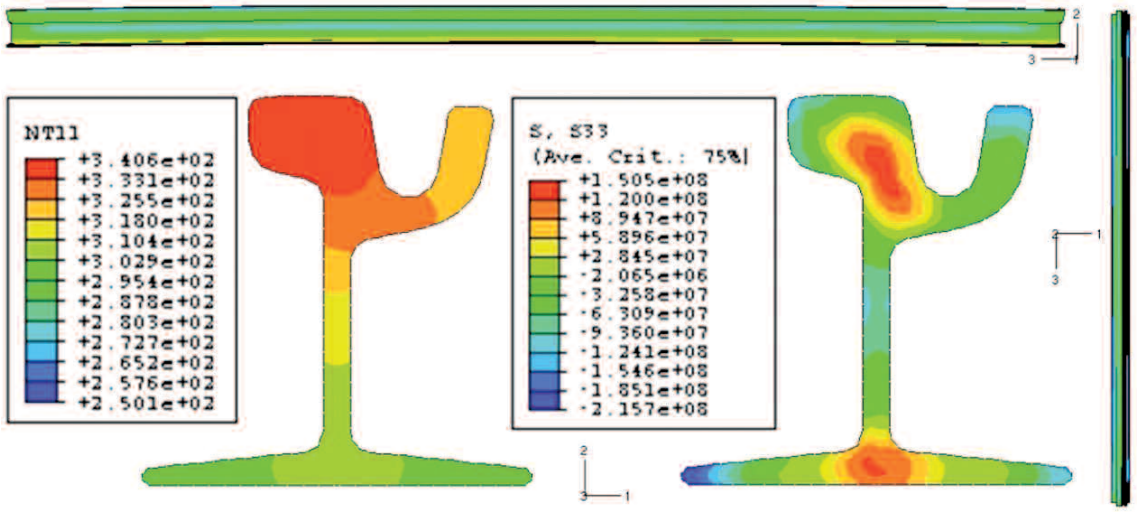

Figure 10. Stresses (S33 in Pa), displacements behavior and temperatures (NT11 in ºC) at time 1623 s.

Figura 10. Tensiones (S33 en Pa), comportamiento de los desplazamientos y temperaturas (NT11 en ºC) a los 1623 s.

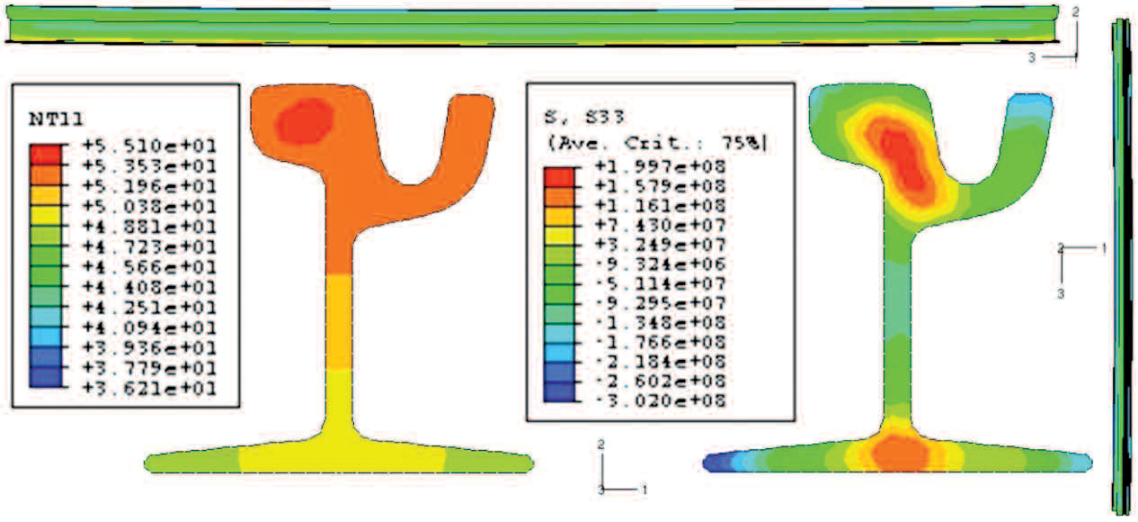

Figure 11. Stresses (S33 in Pa), displacement behavior and temperatures (NT11 in ºC) at final time (t = 10000 s).

Figura 11. Tensiones (S33 en Pa), comportamiento de los desplazamientos y temperaturas (NT11 en ºC) al final del enfriamiento (t = 10000s).

6. SELECTING COOLING STRATEGIES

This section compares the longitudinal residual stresses generated during both configurations of the rails on the cooling bed: vertical (A) and horizontal (B) (see figure 3). Rail-by-rail in a horizontal position is the usual arrangement on cooling beds. It was therefore considered interesting to simulate this configuration and compare it with the results from the models for the vertical position. As a consequence, it would be possible to select the better cooling configuration.

The models were basically the same. The only difference was the position of the rails.

The distribution of the residual stresses at the surface and inside the rail's cross section (at the rail's centre) in position 'B' is displayed in figure 12.

In general terms, there were no major differences at these surface points between rail cooling in either

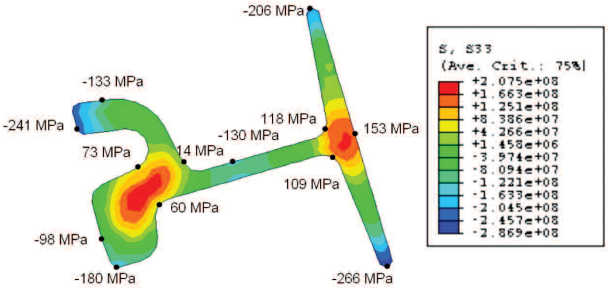

***Figure 12**. Longitudinal residual stresses (S33) for lie down position at the end of the cooling process (t = 10000 s).*

Figura 12. Tensiones residuales longitudinales (S33) para la posición horizontal al final del enfriamiento (t = 10000 s).

of the two positions. Observing figure 13, the biggest differences on the residuals stresses between positions 'A' and 'B' are in points 3 and 6, which present an increment of 66 MPa and 50 MPa, respectively, when cooling in a horizontal position.

Nevertheless, there were appreciable differences along the rail length. Figures 14, 15 and 16 are indicative of this.

S33 behaviour on the big-head-surface (Fig. 14) was more uniform along the rail when cooling in a vertical position. However, the compression magnitudes were higher than in the horizontal position (with a maximum difference between both positions of 18.5 MPa).

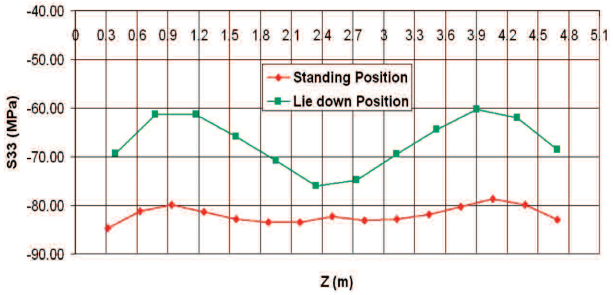

Figure 14. Residual stresses on the rail's big-head-surface, along the rail's length.

Figura 14. Tensiones residuales en la superficie de la cabeza mayor del raíl, a lo largo del raíl.

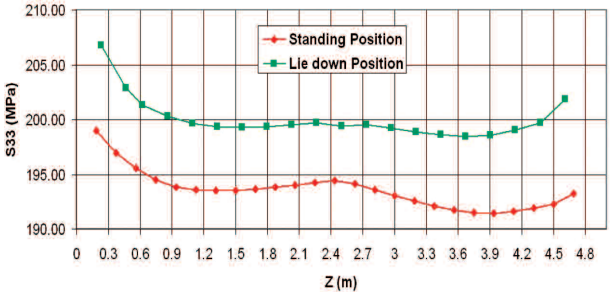

Figure 15. Residual stresses at the rail's big-head-center, along the rail's length.

Figura 15. Tensiones residuales en el centro de la cabeza mayor del raíl, a lo largo del raíl.

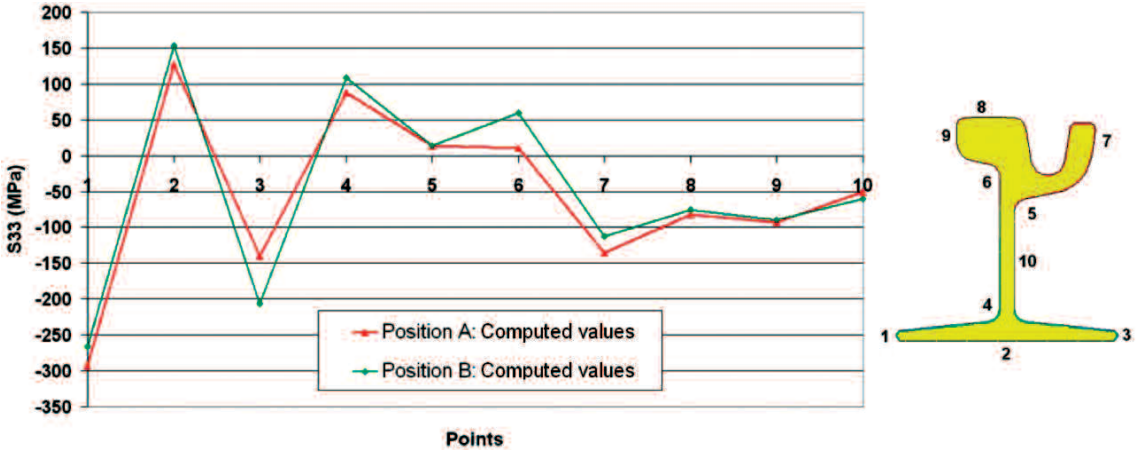

Figure 13. Comparison of computed residual stresses values for 10 interesting surface points for both positions at the end of the cooling process (t = 10000 s). (A) Standing and (B) Lie down position.

Figura 13. Comparativa de las tensiones residuales calculadas para 10 puntos de interés de la superficie para ambas posiciones al final del enfriamiento (t = 10000 s). (A) Posición vertical y (B) Posición horizontal.

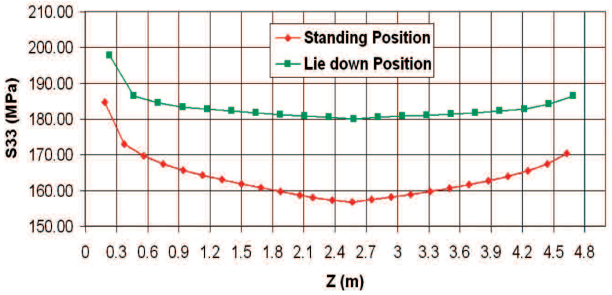

Figure 16. Residual stresses at the rail's base-center, along the rail's length.

Figura 16. Tensiones residuales en el centro de la base del raíl, a lo largo del raíl.

Regarding the inner parts of the rails in both positions, in figures 15 and 16 present the residual stresses of the rail's big-head-centre and base-centre, respectively (which were the points with maximum residual stresses at the end of the cooling process). The maximum difference observed in figure 15 was 8.6 MPa, which is not particularly significant. Nevertheless, in these figures, we can better appreciate the effect of the asymmetrical cooling caused by the wind. The wind blows from the 0m end to the 5m end. Therefore, as the windward part of the rail (0m end) cooled faster than the leeward part and, the windward part developed higher residual stresses. In the case of this 5m rail, the difference between the windward and leeward ends was not so significant (5.72 MPa), but it evidences the effect of the wind (or its consequence: asymmetrical cooling). In larger rails, this difference would be more evident.

Regarding figure 15, there were higher differences in residual stresses between both positions. The maximum difference at the base-centre is recorded at the rail's centre, being 24 MPa. The higher difference can be explained because during the cooling the base-center cools down slower in vertical position than in horizontal positions, where the base of the rail is freer to radiate its heat to the ambient.

As a result, certain differences were evident in residual stresses by cooling the rail in a vertical or horizontal position. It seems that cooling in a horizontal position develops higher residual stresses.

7. CONCLUSIONS

The cooling process for the grooved rail (Ri60) on an indoor cooling bed was modelled and simulated using FLUENT® and ABAQUS® software. The models included the boundary conditions presented in the real plant (wind direction and magnitude). An advantage of using CFD software was that there was no need to specify the film heat transfer coefficient or view factors to simulate the process, as FLUENT® calculates them from the rail's properties (geometry, material and temperature) and the surrounding conditions. This would be specially complicated to establish 'manually' in this case of cooling by forced convection.

In the proposed methodology, the cooling curves (temperature-time) for each element of the thermal model were used to determine the thermal expansion coefficient at each iteration. In this way, the stresses and displacement were simulated in a more realistic way, as they consider the face transformation of the studied steel.

The results from the thermal and stress/displacement models were compared with the experimental values available, and there was good correspondence. The simulations showed the formation of the residual stresses along the time and explained the final bending observed in the real plant.

Two cooling configuration strategies were simulated and compared: cooling in vertical position and cooling in horizontal position. There were differences in the residual stresses obtained in both configurations. The tendency seems to indicate that the horizontal position is the configuration giving higher residual stress values.

Currently the research group is studding the effect of input section's temperature, stresses and bending, on the straightening process. It seem that there is a suited temperature at which the section must be straightened in order to reduce residual stress and bending after this process.

8. Acknowledgments

The authors thank the Research Fund for Coal and Steel (RFCS) for its financial support for the projects RFS-CR-04023, RFS-CR-04043, RFS-CR-03012 and RFS-PR-06035. Also we would like to thank PhD. Maag and PhD. Eisenkolb for the valuable discussions and the experimental data provided. We are grateful to the "Dirección General de Investigación" of the Spanish Ministry of Science and Innovation for the financial support of the projects DPI2006-03060, DPI2006-14784, DPI-2006-02454 and DPI2007-61090.

Finally, the authors also thank the Autonomous Government of La Rioja for its support through the 3º Plan Riojano de I+D+i.

List of symbols

L	Segment length
N	Number of divisions of the segments
$NT11$	Temperature [°C]
S	Stress [Pa]
$S33$	Longitudinal stress [Pa]
T	Temperature [°C]
α_{th}	Thermal expansion coefficient [°C^{-1}]
$\alpha_{th,ferrite}$	Thermal expansion coefficient due to the ferrite [°C^{-1}]
$\alpha_{th,austenite}$	Thermal expansion coefficient due to the austenite [°C^{-1}]
χ	volume fraction of intended phase at T temperature [%]
χ_0	volume fraction of intended phase at transformation termination [%]
T_s	Transformation start temperature [°C]
T_f	Transformation end temperature [°C]
t	time [s]

9. REFERENCES

[1] J. Szalai, *Overall sensitivity analysis if hot-rolled beam-columns*, in: *Metal structures: design, fabrication, economy*, Millpress, Rotterdam, 2003.
[2] O. Orringer, W. Paxont, D. Gray and P. Raj, *Int. J. Sci. Tech. Friction, Lubrication and Wear* 191 (1996) 25-34.
[3] J. Ringsberg and T. Lindbäck, *Int. J. Fatigue* 25 (2003) 547-558.
[4] J.T. Maximov, T.V. Kuzmanov, A.P. Anchev and M.D. Ichkova, *J. Mater. Process. Technol.* 171 (2006) 459-466.
[5] S. Serajzadeh and S.M.H. Mirbagheri, *Ironmaking Steelmaking* 35 (2008) 115-123.
[6] J.B. Ordieres, A.G. Marcos, J.A. González and V.L. Rubio, *Ironmaking Steelmaking* 31 (2004) 43-50.
[7] J.B. Ordieres, V. Torre-Suárez, A.V. Pernía-Espinoza and A. González-Marcos, *Rev. Metal. Madrid* 44 (2008) 29-38.
[8] P.J. Webster, X. Wang and G. Mills, Proc. NATO *Advanced Research Workshop on Measurement of Residual Stress using Neutron Diffraction*, Oxford, *Kluwer Academic Publishers*, 1992, 517-524.
[9] E. Ardelean, M. Ardelean, A. Socalici and T. Heput, *Rev. Metal. Madrid* 43 (2007) 181-187.
[10] A. Ramírez, A. Mosqueda, V. Sauce, R. Morales, A. Ramos and G. Solorio, *Rev. Metal. Madrid* 42 (2006) 209-215.
[11] P. Besuner, *Fracture mechanics analysis of rail with shell-initiated transverse crack, Rail Steels-Developments, Processing and Use*, ASTM STP 644, 1978, pp. 303-329.
[12] O. Orringer, *Crack propagation life of detail fracture in rails*, Volpe National Transportation System Center, report no. DOT/FRA/ORD-88/13, October, 1988.
[13] H. Yoshida, *Trans. ISIJ* 24 (1984) 401-407.
[14] M. Abouaf, J.L. Chenot and J.L. Marcelin, *Int. J. Num. Meth. Eng.* 19 (1983) 1453-1465.
[15] J.L. Marcelin, M. Abouaf and J.L. Chenot, *Comp. Meth. Appl. Mech. Eng.* 56 (1986) 1-16.
[16] O. Zienkiewicz, S. Valliapan and I. King, *Int. J. Num. Meth. Eng* 1 (1969) 75-100.
[17] G. Comini, S.Del Guidice, R. Lewis and O. Zienkiewicz, *Int. J. Num. Meth. Eng.* 8 (1974) 613-624.
[18] F.D. Fischer, E. Hinteregger and F.G. Rammerstorfer, *A computational study of the residual stress distribution in thermally loaded beams of cross-section on frictional support*, in: Non-linear Comp. Mechanics, State of the Art, Springer, Berlin, 1991, pp. 737-750.
[19] J. Basu, S.L. Srimani and D.S. Gupta, *J. Strain Analysis Eng. Design* 39 (2004) 15-24.
[20] I.I. Boyadjiev, P.F. Thomson And Y.C. Lam, *J. Mat. Process. Tech.* 147 (2004) 268-275.
[21] Fluent® User's guide, version 6.3, Fluent Incorporated, 2006.
[22] I.I. Boyadjiev, P.F. Thomson and Y.C. Lam, *ISIJ Int.* 36 (1996) 1413-1419.
[23] S. Kamamoto, T. Nishimori and S. Kinoshita, *Mater. Sci. Technol.* 1 (1985) 798-804.
[24] E. Fink and K. Pratt, *Data Mining In Time Series Databases* M. Last, A. Kandel, and H. Bunke (Eds.), 2004, pp. 43-64, World Scientic.
[25] Abaqus Analysis User's Manual version 6.7, 2005.